a

University of Colorado Boulder

ASEN 2002: Introduction to Thermodynamics/Aerodynamics

Aerodynamics of a Cambered Airfoil

Authors:

A. Alameri, F. Greer, S. D'Souza, T. Slack, N. Portman

(Section 11 Group 14)

December 12, 2018

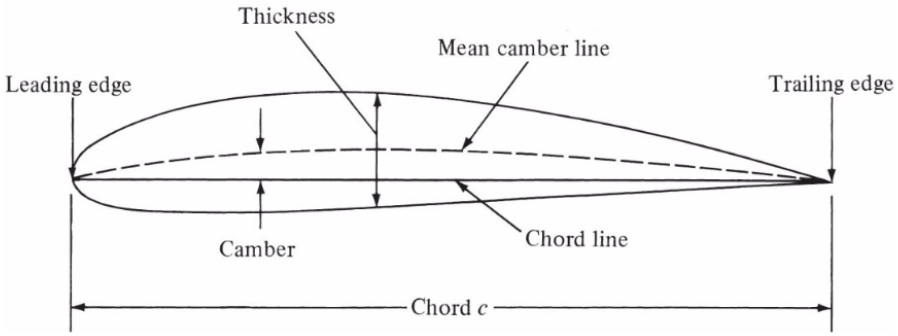

Fig. 1 Cambered Airfoil

This lab investigated a Clark Y-14 airfoil in a low-speed wind tunnel to study how the pressure distribution on a body in a flow leads to the aerodynamic forces acting on that body. The pressure coefficient, C_p, was studied in order to examine this pressure distribution. It was seen that a feature of C_p over the airfoil was a larger negative value on top of the airfoil, which illustrates how the pressure distribution creates lift. An analysis of how this pressure distribution varied over different velocities and angles of attack yielded relationships between the coefficient of lift on the airfoil, the coefficient of drag, and the angle of attack. Important aspects of these relationships were able to be examined, such as how the coefficient of lift increased with the angle of attack until a certain limit, where the coefficient of lift decreased rapidly due to a stalling effect. The maximum coefficient of lift was found to be dependent on the angle of attack and the airspeed. Similarly, it was seen that the coefficient of drag increased with the angle of attack. Lastly, the relationships that were obtained in this lab were also seen to be approximately compatible with those in the official NACA graphs for the Clark Y-14 airfoil shown in Figure 12.

I. Nomenclature

C_p	=	Pressure Coefficient
q_∞	=	Dynamic pressure
P_{local}	=	Local pressure
P_∞	=	Free stream pressure
ρ_∞	=	Density of free stream
V_∞	=	Velocity of free stream
P_{atm}	=	Atmospheric pressure
R	=	Gas constant of air
T_{atm}	=	Atmospheric Temperature
C_d	=	Drag Coefficient
C_l	=	Lift Coefficient
C_m	=	Moment Coefficient
α	=	Angle of Attack
C_n	=	Normal force Coefficient
C_n	=	Axial force Coefficient
C	=	Chord length

II. Introduction

An airfoil is a representation of the geometry of the cross section of a wing. This simple representation of a wing is critical to the analysis of the aerodynamic forces on an aerodynamic body because it allows the problem to be reduced to two dimensions. Furthermore, it is known that all of the aerodynamic forces that act on a body in a flow are only a result of the pressure and shear-stress distributions on the body. The focus of this lab is to investigate the pressure distribution on an airfoil in a wind tunnel and deduce its effects on lift and drag. The airfoil that was studied is a cambered Clark Y-14 airfoil, which has been outfitted with an array of pressure taps to understand the distribution of pressure on the surface of the airfoil under different flow conditions. The general geometry of this airfoil can be seen in Figure 1, and the specific shape is described by a list of measurements of the features, such as the chord length and width of the airfoil at locations along the chord. Analyzing the distribution of pressure on this airfoil showed how the aerodynamic forces originate and change with airspeed and angle of attack.

III. Experimental Setup and Measurement Techniques

In this lab the measurements were performed using a rectangular Clark Y-14 airfoil that spans the entire wind tunnel test section (i.e. assuming it is an infinite wing). It was assumed that all three-dimensional effects could be ignored, so that the flow could be treated as purely two-dimensional. This means that the airspeed and pressure could be treated as equal at each spanwise location on the airfoil; these values will only change as a function of distance in the direction of

flow. Therefore, all of the measurements were taken at a single location on the airfoil (at about 50% of the span to avoid the boundary layer effects caused by the wind tunnel walls).

At this location on the airfoil, nineteen pressure taps were mounted along the surface of the airfoil that measured the differential pressure between the freestream static pressure in the wind tunnel and each port on the airfoil. Measurements were taken via a Scanivalve DSA3217 Multi-Port Pressure Scanner. The location of these ports on the cross section can be seen in Figure 2. This technique of pressure measurement has some limitations. Notably, The pressure scanner

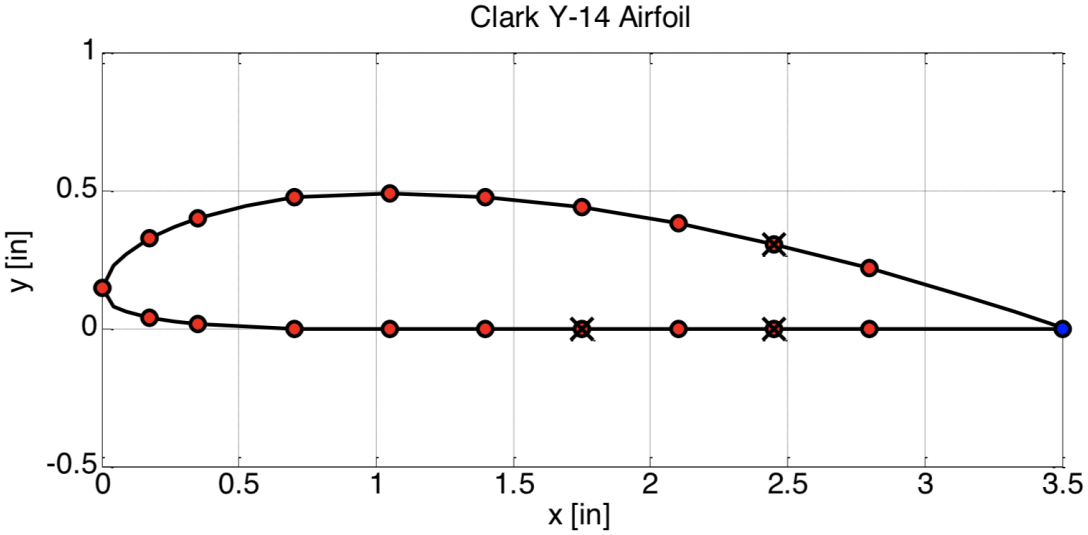

Fig. 2 Location of Pressure Ports on the Clark-Y14 Airfoil

used in this lab only had 16 inputs, so it was required that ports 9, 13, and 15 must be omitted from testing. Similarly, there are physical limitations of fitting a port to the trailing edge of an airfoil, so the pressure at this point was linearly interpolated from other measurements. Specifically, this value was found by taking the average of the values obtained by linearly interpolating from the last two ports on both the top and bottom of the airfoil. These omissions can be seen in Figure 2: the crossed-out ports are omitted, and the blue port at the trailing edge is obtained through linear interpolation.

With the pressure measurements thus set up, and the ability to receive airspeed and dynamic pressure data from the wind tunnel, measurements were taken analyze the aerodynamic forces on this airfoil. Specifically, measurements were taken at angles of attack of -15, -7, 1, and 9 degrees and at velocities of 9, 17, and 34 m/s at each angle. Other groups performed measurements at other angles of attack, creating a complete data with a range of angles of attack from -15 degrees to 16 degrees, each one measured at airspeed velocities of 9, 17, and 34 m/s. A comprehensive analysis of all the groups' measurements was needed to understand the behavior of the airfoil for this range of angles of attack and velocities.

IV. Post-processing and Calculation of Force Coefficients

Once the raw data points were obtained and stored, a routine to import the data and sort them was established. Using equation 1, the coefficient of drag was calculated. The data file provided all the terms in the equation, where q_∞ readings were given by the pitot-static tube configuration. The numerator of equation 1, i.e. the difference between the local pressure and the free-stream pressure, was given by the Scanivalve DSA3217 Multi-Port Pressure Scanner. In other words, each of the red ports in figure 2 was connected to a Scanivalve DSA3217 Multi-Port Pressure Scanner, and each gave a differential pressure reading referenced to the free stream pressure.

Once the coefficients of pressure were determined, a numerical integration was done to get the coefficients of drag and lift. This was done by assuming that between each port, the pressure coefficients are constant. This assumption does not introduce much error in this case, because the difference between each port is not large. However, this error also depends on the speed. Higher speeds will yield higher difference in pressure, and thus this assumption might lead to noticeable errors.

The numerical integration first found the coefficients of normal and axial forces, which take the axis of calculations to be with respect to the resultant force obtained from the integration between the ports. Once the coefficients of axial and normal forces were determined, they were converted to coefficients of lift and drag using simple geometry. Equation 3, and 4 explain how this numerical integration was accomplished. Equation 5 and 6 show how the coefficients of lift and drag were obtained. Those equations demonstrate that part of the pressure force contributes to lift and part contributes to drag. The magnitude of the contribution is dependent on the angle of attack.

$$C_p = \frac{P_{local} - P_\infty}{q_\infty} = \frac{P_{local} - P_\infty}{0.5\rho_\infty (V_\infty)^2} = \frac{P_{local} - P_\infty}{0.5(\frac{P_{atm}}{RT_{atm}})(V_\infty)^2} \tag{1}$$

$$\vec{V}_\infty = \sqrt{2\Delta P(\frac{RT_{atm}}{P_{atm}})} \tag{2}$$

$$C_n = -\sum_{i=1}^{n} \frac{1}{2}(C_{pi} + C_{pi+1})\frac{\Delta x_i}{C} \tag{3}$$

$$C_a = \sum_{i=1}^{n} \frac{1}{2}(C_{pi} + C_{pi+1})\frac{\Delta y_i}{C} \tag{4}$$

$$C_l = C_n cos\alpha - C_a sin\alpha \tag{5}$$

$$C_d = C_n sin\alpha + C_a cos\alpha \tag{6}$$

Ideally, a more detailed error analysis would take into consideration all sources of errors. One of they key things to notice is that all of the errors in the coefficients of lift and drag are mainly coming from the coefficient of pressure. Equations 1 and 2 tell show where the errors in the coefficients of pressure might come from. It is important to note that only the systematic errors where considered, it was assumed that the individual data points do not have error, and the only error comes from the instruments. From equation 1, there are four types of errors. Firstly, the differential pressure obtained from the Scanivalve DSA3217 Multi-Port Pressure Scanner, which has an error of 0.20% of the full scale [4]. The second and third source of error are from calculating the free-stream density, which can be calculated via the Ideal Gas Law. Treating the specific gas constant as an exact number, the only two sources of error will then be Atmospheric temperature, and Atmospheric Pressure. According to Lab 3, from CU'S Fall 2018 ASEN 2002 [3], the systematic error for the atmospheric pressure measurement devices is 1.5% of the full span, and hence the error is 3450 Pa. This indeed will drive the error calculations up for it is a very huge number. Notably. this error decreases with higher speeds [3]. On the side of Atmospheric temperature, the error from the same lab document [3] is taken to be 0.25 Kelvin. Lastly, the last source of error would be from the free-stream velocity, which is given by equation 2. The Airspeed values were determined by a pitot-static tube set-up. The same values and procedure that was done in equation 1 was used for the uncertainties in T_{atm} and P_{atm} . The difference in pressure values were obtained via an airspeed differential pressure transducer. According to Lab 3 document [3], the error is 1% of the full span for the airspeed differential pressure transducer.

It is important to note that the last port at the trailing edge, which is at 3.5 inches from the leading edge, as seen in figure 2, does not have a port to measure the pressure differential at, as described in Section III. Hence, the values at the bottom and the upper half of pressure coefficient for the last two ports before the trailing edge were linearly extrapolated to get a value at the trailing edge. Once two values for the pressure coefficients at the trailing edge were obtained from the upper and lower half's of the cross section of the air foil, the values where averaged. Hence, the error values from the upper and lower will also have a contributions from each half. The error for the trailing edge was calculated from the equations of error for measured values given by the "Introduction to Error Analysis" book [2].

This approach of linear extrapolation might not be the most optimal approach simply because it is not the case that the relationship between coefficients of pressures are linear as you move on the airfoil. This approach might be only valid if the distances between the ports and the trailing edge are small, so the relationship becomes more linear.

However, in this lab, it was advised to use the maximum and minimum values for each coefficient of pressure as the bounds for the error. Figures 3,4,8, and 9 show the pressure coefficient values with error bounds. Notably, it is known that pressure coefficients positive values should not exceed 1, however they can for the negative values. Some of error bound values exceed 1 on the positive side, however this might be due because this is an variance bounds nor the

absolute errors, and hence some individuals data points might have some experimental errors. For the trailing edge values, the mean value of the two maximum and minimum values for both the upper half and the lower half were taken to be the value of the error bound on the last port.

Lastly, there were some out-layers that were excluded. Table 1 in Appendix states the data that were excluded and the reason of exclusion.

V. Airfoil Static Pressure Coefficient Distribution

Once the data have been properly normalized, trends between airspeed and the pressure distribution begin to become more noticeable. Figures 3 and 4, as well as Figures 8 to 11 in the Appendix shows those trends for various angles of attack and speeds. While it is quite hard to visually determine the maximum points in Figure 3, when blowing the image up and utilizing the data cursor tool in MATLAB, one can see that the pressure distribution is increasing. For a velocity of around 9 m/s, the maximum pressure coefficient at a normalized chord-wise position of 0.2 is -0.6657. If the free stream velocity is increased to around 17 m/s, the pressure coefficient increases to -1.12, and increasing it further to 34 m/s it reaches -1.223. These differences are difficult to observe however, when increasing the scale, one can see that there is a definitive relationship between the two.

This effect can be explained through the utilization of Bernoulli's equation and the design of the Clark y-14 airfoil. The shape of this airfoil has been carefully designed so as to produce lift. In order to generate this lift, there needs to be a pressure difference between the top and bottom of the airfoil. This cambered airfoil has been carefully designed so that the distance the air travels along the streamline along the top, is longer than the distance the air travels along the bottom. Due to the different distances the air travels in equivalent time (i.e. steady flow conditions), the velocity on the top of the airfoil must be higher than the velocity at the bottom of the airfoil. Staying consistent with the assumptions for incompressible flow, Bernoulli's equation can be utilized to show how the pressure distribution is generating the lift of the aircraft.

$$P_1 + \frac{1}{2}(\rho)(V_1)^2 = P_2 + \frac{1}{2}(\rho)(V_2)^2 \tag{7}$$

Rearranging to solve for P_2

$$P_1 + \frac{1}{2}(\rho)(V_1 - V_2)^2 = P_2 \tag{8}$$

Because the Clark Y-14 airfoil is lined with pressure ports along its top and bottom surfaces, the pressure each port measures is dependent on the speed at which the air is flowing over the port. Because of this, the sensors along the top of the airfoil would register a higher velocity, and thus a lower pressure than the sensors would register on the bottom of the airfoil, due to the inverse relationship between V_2 and P_2 in equation 8. This is known as the Venturi tube effect. Because of this difference in pressure is dependent on the velocity registered in the sensor, an increased velocity would register a larger pressure distribution between the top and bottom of the airfoil.

The largest differences along the airfoil chord vary slightly depending on the angle of attack. For most angles of attack, the largest differences between the surface pressures occur earlier or at 0.3 of the chord scale. Generally, these differences stay between 0.1 and 0.2 as in figure 3. In some extreme cases, large negative angles of attack, the largest pressure difference can occur below 0.1 of the chord scale as seen in figure 4. If the angle of attack is increased the center of pressure moves closer to the front of the airfoil. This will in turn increase the value of pitching moment as it is measured from the aerodynamic center of the airfoil, usually around 0.25 of the normalized chord-wise position. The pitching moment highlights the movement of the aircraft as if there is a large negative angle of attack, this large pitching moment is acting up generating a positive lift force even as the aircraft is angled down, counter intuitive to what one might naturally think. If there is a large positive angle of attack the value of this pitching moment is going to be slightly less as it is acting closer to the aerodynamic center however the lift generated is still acting up. This shows why it is hard to recover from stall. Once the aircraft reaches the critical angle of attack this pitching moment is also forcing the nose of the aircraft up making it harder to recover from stall. In other words, as the angel of attack increases, the airfoil generates more lift, and the pressure distribution changes. This change can be seen for instance in figure 8 with angel of attack of 1 degree, compared to figure 9 with an angel of attack of 9 degrees. It can be seen that in figure 9 the maximum pressure distribution difference is shifted to the leading edge, and it has a higher value, and hence higher lift. This also means that the adverse pressure gradient the flow has to overcome increases, and hence stall and flow separation happens at earlier locations on the air foil.

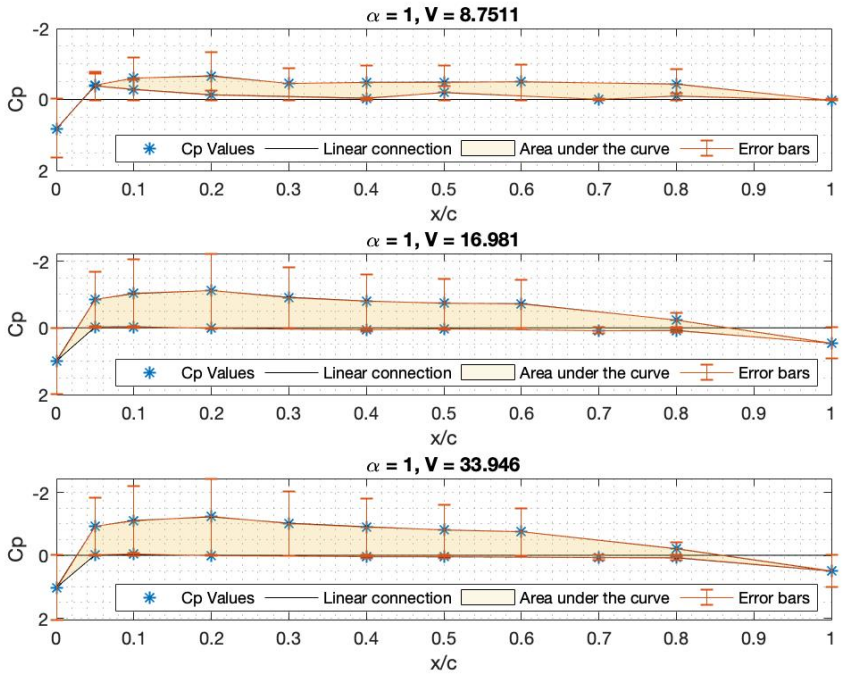

Fig. 3 Pressure coefficient versus normalized chord-wise position for different velocities at an angle of attack of 1 degree

Flow separation can be determined from the slope of the pressure distribution across the length of the chord from the top of the airfoil. This can be seen when comparing figure 3 and 4. In figure 3, the pressure coefficient on the top of the airfoil is linearly decreasing for most of the chord length. This is due to the angle at which the airfoil was placed in the wind tunnel and for figure 3, at an angle of attack of 1 degree, this variable slope makes sense as the pressure coefficient would change as the shape of the chord is changing. In the pressure distribution at 9 meters per second at an angle of attack of negative 15 degrees (figure 4), the pressure coefficient of the top of the airfoil is changing. If the speed is increased to 34 meters per second, the slope of the coefficient of pressure is constant after a certain point. This constant pressure distribution is consistent with flow separation, as the pressure is no longer changing due to the chord shape.

This constant pressure is consistent with flow separation. Before separation occurs, the ports measure a given pressure value across their opening, once the flow begins to separate away from the wing, these ports cannot measure the pressure of the moving air. The readings they give is the ambient pressure which is constant for the rest of the wing.

Because group 14 only measured the pressure distribution for an angle of attack of 1 degree, additional groups must be consulted to determine how this pressure distribution will vary with changes to angle of attacks at a low angle. Once all the data was compiled, it became evident that as the angle of attack increased, the largest difference in surface pressure began to occur closer and closer to the nose of the airfoil. However the slope of the top of the pressure distribution still changes, showing the flow had not yet separated for smaller angles of attack.

VI. Lift and Pressure Drag Coefficients

The plots of angle of attack versus coefficient of lift can be seen in the top left plot of figures 5, 6, and 7. The graph at 17 m/s and 34 m/s show the most clear relationship of angle of attack to lift coefficient. In these graphs between -5 degrees and 5 degrees there is a linear increasing relationship between the angle of attack and lift coefficient. This relationship is consistent with the NACA report of the airfoil seen in figure 12 [1]. At extreme angles of attack (about -10 and 10) there is sharp drop off of the lift coefficient this is characteristic of an aerodynamic stall. The angle of attack that the stall occurs at is dependent on the airspeed of the wing. At 34 m/s stall occurs at 10 degrees where as at 17 m/s stall occurs around 5 degrees. At 9 m/s the graph does not have a sharp drop off but there is a decrease in rate of change

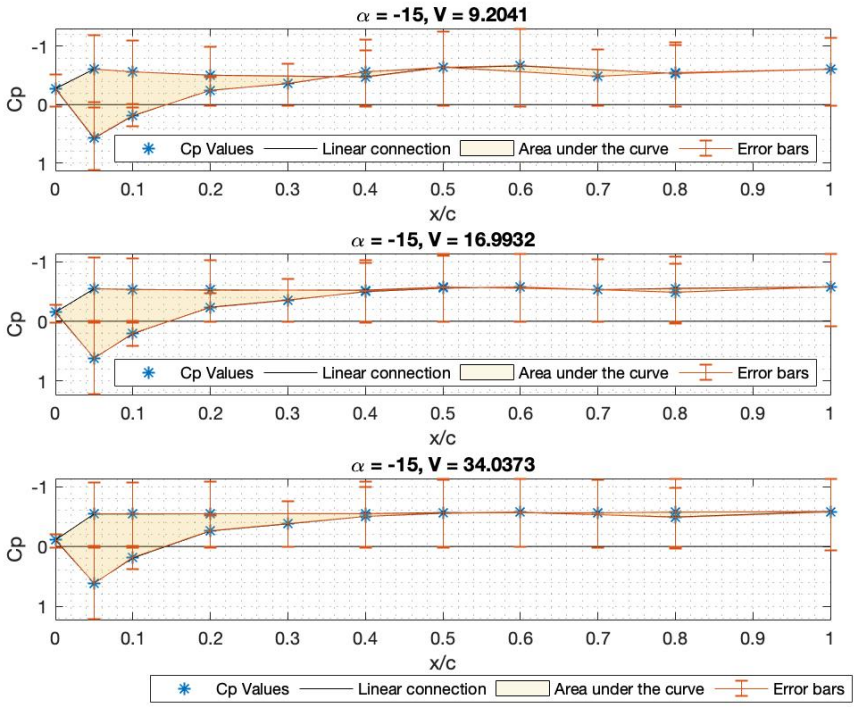

Fig. 4 Pressure coefficient versus normalized chord-wise position for different velocities at an angle of attack of negative 15 degrees

of the coefficient of lift that happens around 5 degrees. From these graphs it is evident that an aerodynamic stall is dependent on the angle of attack and airspeed.

The maximum coefficient of lift generated by the Clark Y-14 airfoil is about 1.5, at 10 degrees angle of attack and 34 m/s. The maximum possible coefficient of lift is dependent on velocity. Specifically it decreases with a decrease in velocity. For instance at 17 m/s the $C_{L,max}$ is only around 1.15 and at 9 m/s is only about 0.75.

Another interesting behavior of the Clark Y-14 airfoil is that it exhibits a non-zero coefficient of lift at zero degrees angle of attack. At 34 m/s the coefficient of lift is around 0.5 at zero degrees angle of attack. This is because the airfoil is not symmetric. The bottom side is flat and the top is curved. The coefficient of lift equals zero at around -5 degrees angle of attack for 34 m/s.

Overall this lab's graphs of angle of attack and coefficient of lift and drag match fairly well with the NACA graphs. A few major inconsistencies are the length of the linear relationships and the amount of drop off. The lab's linear relationships do not extend as far as the NACA ones. Additionally the NACA graphs only drop off to a c_L of about 1.2 where the Lab's drop off to around 1. These inconsistencies could stem from errors in the measurements and the fact that the NACA graphs show an airspeed of 21 m/s where as the Lab's graphs are only 9,17,34 m/s which makes a direct comparison impossible. Without measurements taken at the same airspeed it is difficult to make any comparisons between the NACA graphs and the Lab's graphs without making large assumptions. Taking measurements at the same speed and the same testing conditions would insure that there is almost the same results. In other words, matching Mach Number and Reynolds numbers for the free-stream conditions is necessary to have the same results for the same aerodynamic shape regardless of the scale. Furthermore, the configuration of the wind tunnel itself might affect the results obtained. Due to the small size of the test section relative to the airfoil, it is very likely that there was some edge effects from the wind tunnel itself. In fact in figure 12 the NACA graph states that their data was "corrected for tunnel-wall effect" meaning that their data was most likely more accurate. The listed Reynolds number on the NACA graph was 3.02e6 where as the lab's Reynolds numbers were between 4.4e4 and 1.7e5 [5]. This large difference in the Reynolds number greatly effects the coefficient of lift. Matching the lab's Reynolds number to the NACA Reynolds number by increasing the velocity of the wind tunnel would cause the lab's data to be closer to the NACA values. The Reynolds number could be changed to match the NACA value by testing at a higher airspeed or creating a larger scall

wing with a longer cord length. This lower Reynolds number in the lab also can explain why the data seems to suggest that stall is dependent on angle of attack and velocity. As reported in the NASA Contractor Report 4745 Reynolds number has an effect on the stall characteristics of an airfoil [6]. In real world conditions, with a wing with standard roughness and an average Reynolds number, the aerodynamic stall is only dependent on the angle of attack.

VII. Conclusion

This lab has reviewed and studied the pressure difference and flow dynamics over a Clark Y-14 airfoil in a low-speed wind tunnel at 3 different free stream velocities; 9, 17, and 34 m/s and various angles of attack from -15 to 16 degrees.Through testing and data collection, in conjunction with calculating aerodynamic forces acting on the airfoil, the processing of the data shows and generally agrees with known NACA values of the Clark Y-14 airfoil.

The pressure differences generated through different velocities as well as angles of attack shows the ability and flight characteristics of the Clark Y-14 airfoil. In general, it can be seen that as the velocity increase, more differential pressure is obtained, and hence, more lift. On the other hand, as angel of attack increases, not only more lift is generated, but stalling happens earlier.

Though the testing is done in a scaled down variant, this data is applicable to a full scaled up version for practical use, as long as Reynolds numbers and Mach number for the free-stream conditions are matched. This scaling works with identical geometry bodies that are linear scales of one another, and as long as they are tested at the same free stream Reynolds number and mach number.

This style of testing and analysis can be applied to any number of aerodynamic bodies in order to understand the different flight characteristics and maximum conditions that they can endure. This makes it possible for any designer to decide what geometry a given airfoil needs to have in order to work in practical applications. However, notably, this testing method has some limitations that might limit its applications, especially when we it comes to looking at the trailing edge. Put it differently, although this method achieved a very good level of matching to the official NACA 628 report in terms of pressure, drag, and lift coefficients, it was mainly limited by the physical locations of the ports, where it is impossible to measure the pressure at the trailing edge, and hence other method of estimations must be considered.

References

[1] Pinkerton, R. M., and Greenberg, H., "Aerodynamic Characteristics of a Large Number of Airfoils Tested in the Variable Density Wind Tunnel," National Advisory Committee for Aeronautics, vol. 628, 1938, p. 36.

[2] Taylor, J. R., "General Formula for Error Propagation," An Introduction to Error Analysis: The Study of Uncertainties in Physical Measurements, 2nd ed., University Science Books, Sausalito, CA, 1996, pp. 73–78.

[3] ASEN Department, "Aerodynamics Experimental Laboratory 1:Calibration of the ITLL Low-Speed Wind Tunnel," ASEN 2002 Lab Document (not yet published).

[4] ASEN Department, "Aerodynamics Experimental Laboratory 2: Aerodynamics of a Cambered Airfoil," ASEN 2002 Lab Document (not yet published).

[5] "Reynolds Number Calculator," Airfoil Tools Available: http://airfoiltools.com/.

[6] Polhamus, E. C., "A Survey of Reynolds Number and Wing Geometry Effects on Lift Characteristics in the Low Speed Stall Region," NASA Contractor Report 4745, Jun. 1996.

Appendix

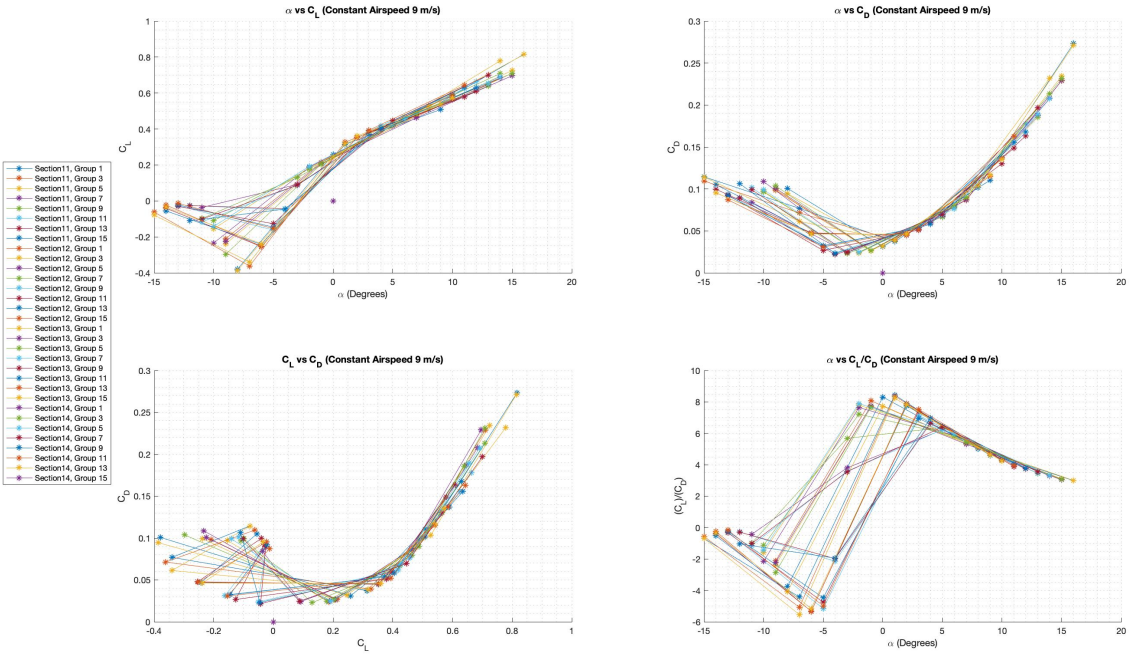

Fig. 5 Graphs of angles of attack and Coefficients of lift and drag for 9m/s.

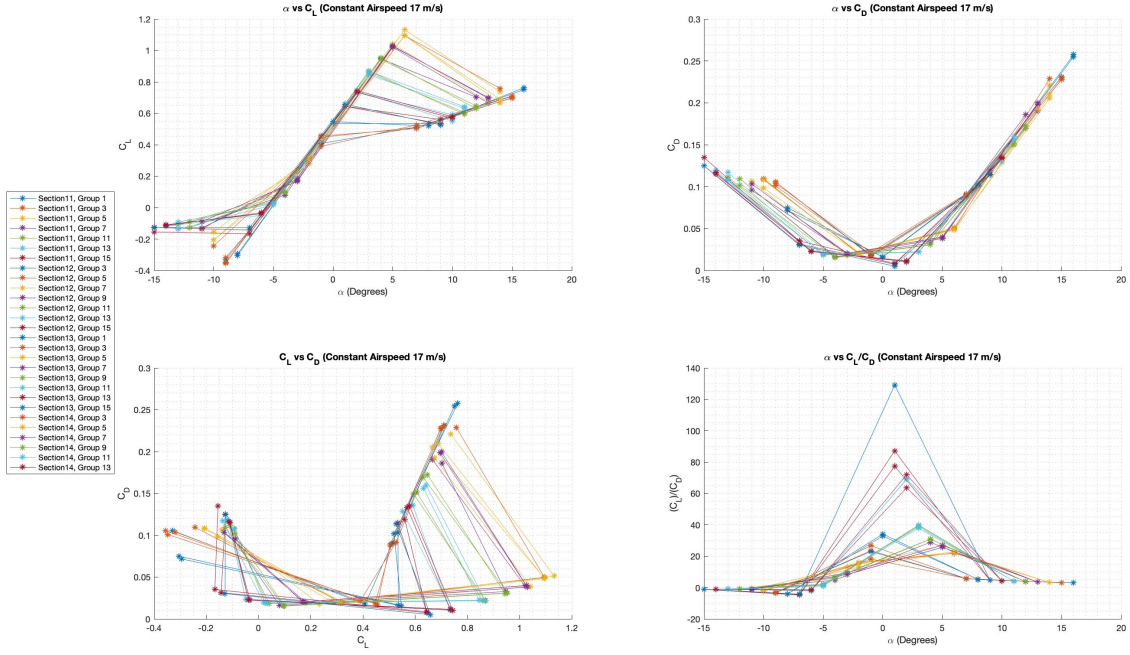

Fig. 6 Graphs of angles of attack and Coefficients of lift and drag for 17m/s.

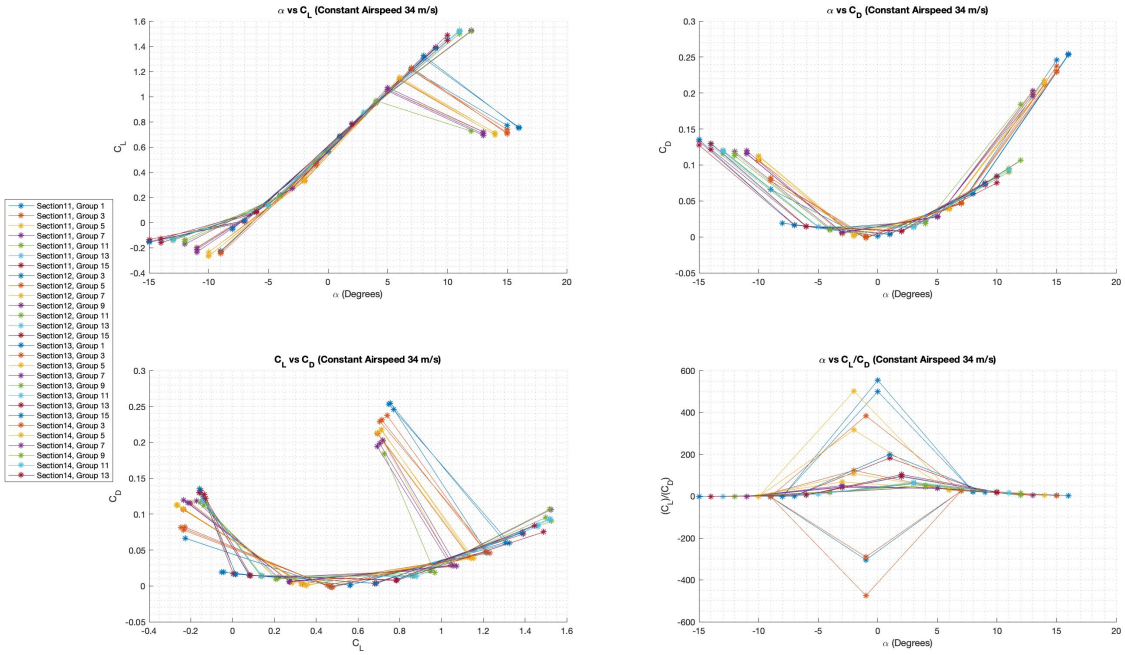

Fig. 7 Graphs of angles of attack and Coefficients of lift and drag for 34m/s.

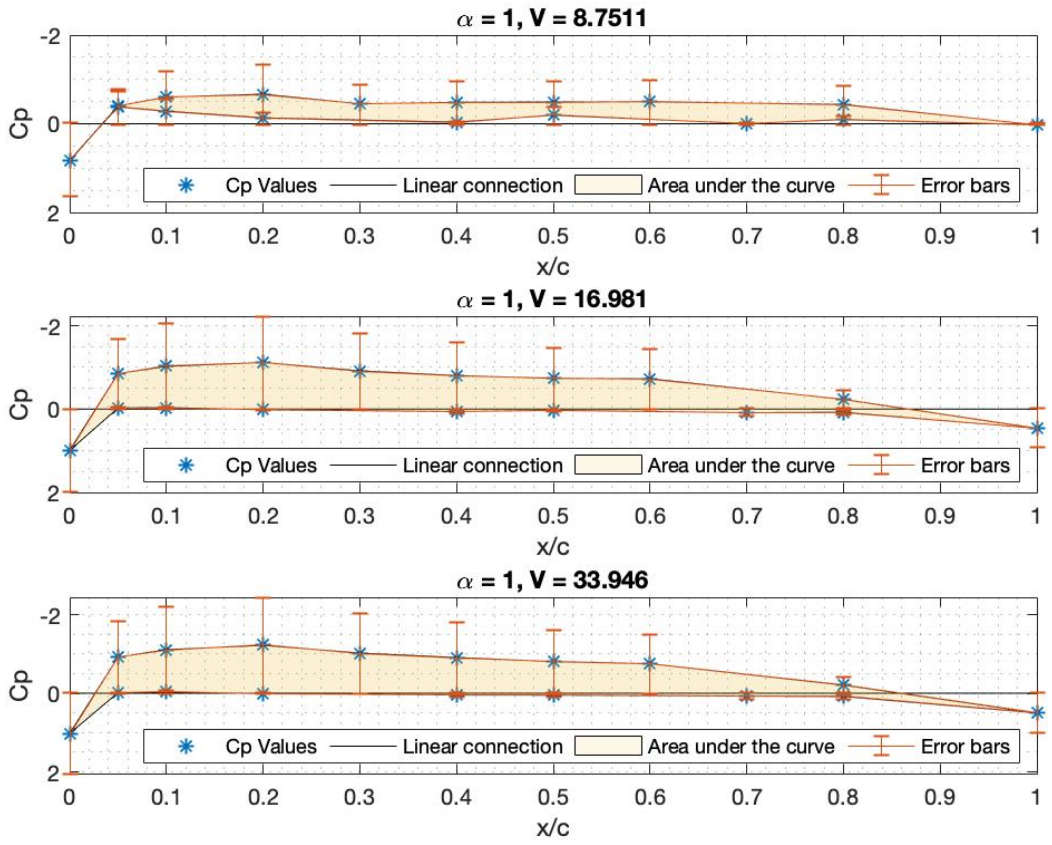

Fig. 8 Pressure coefficient versus normalized chord-wise position for different velocities at an angle of attack of 1 degree

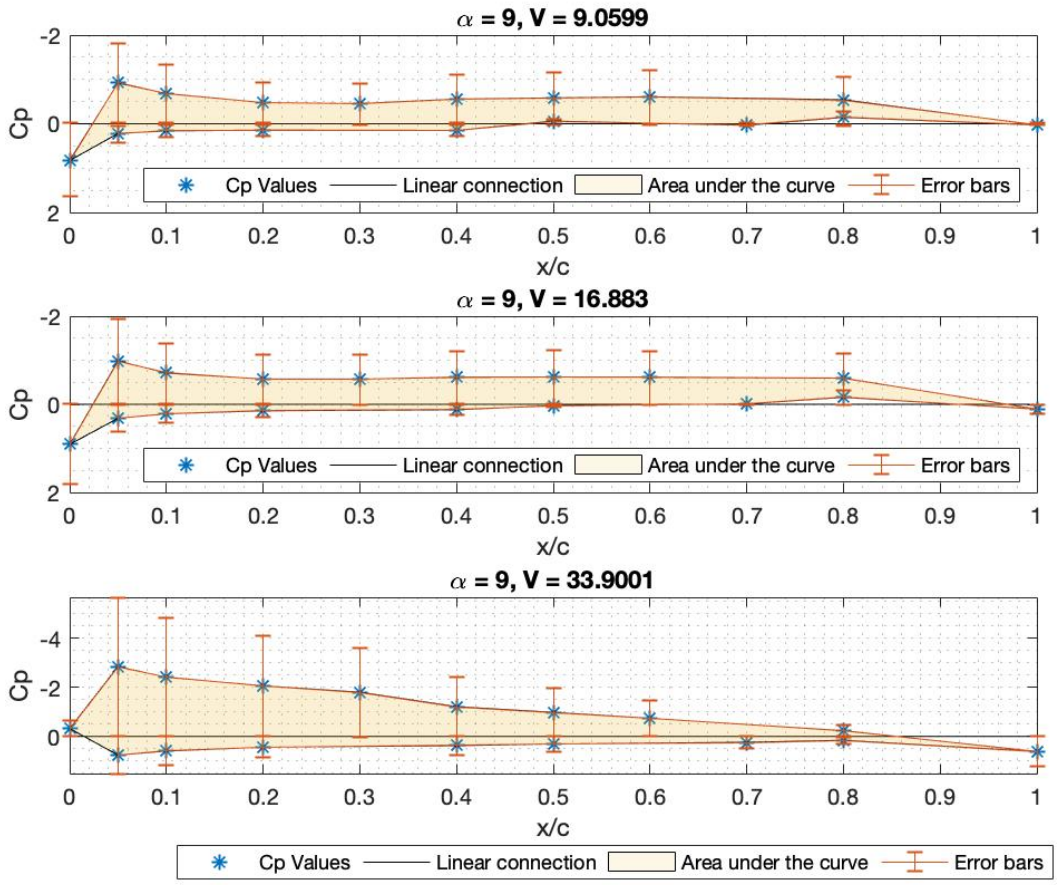

Fig. 9 Pressure coefficient versus normalized chord-wise position for different velocities at an angle of attack of 9 degrees

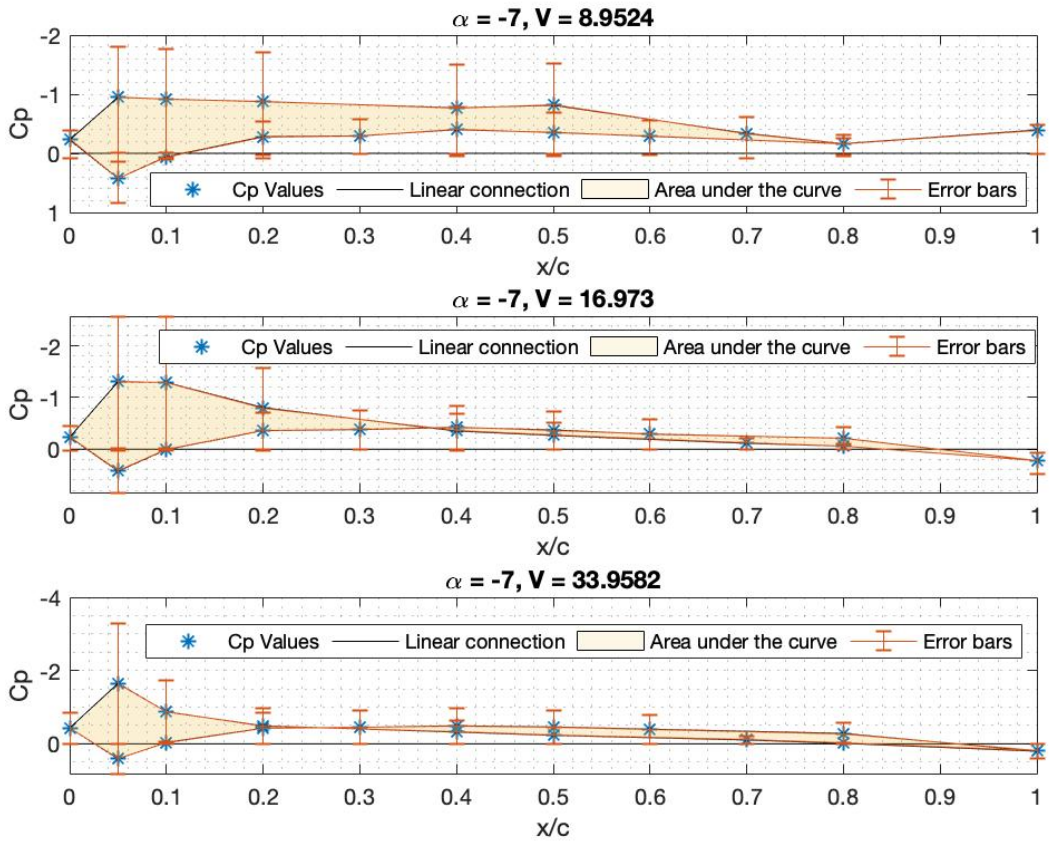

Fig. 10 Pressure coefficient versus normalized chord-wise position for different velocities at an angle of attack of negative 7 degrees

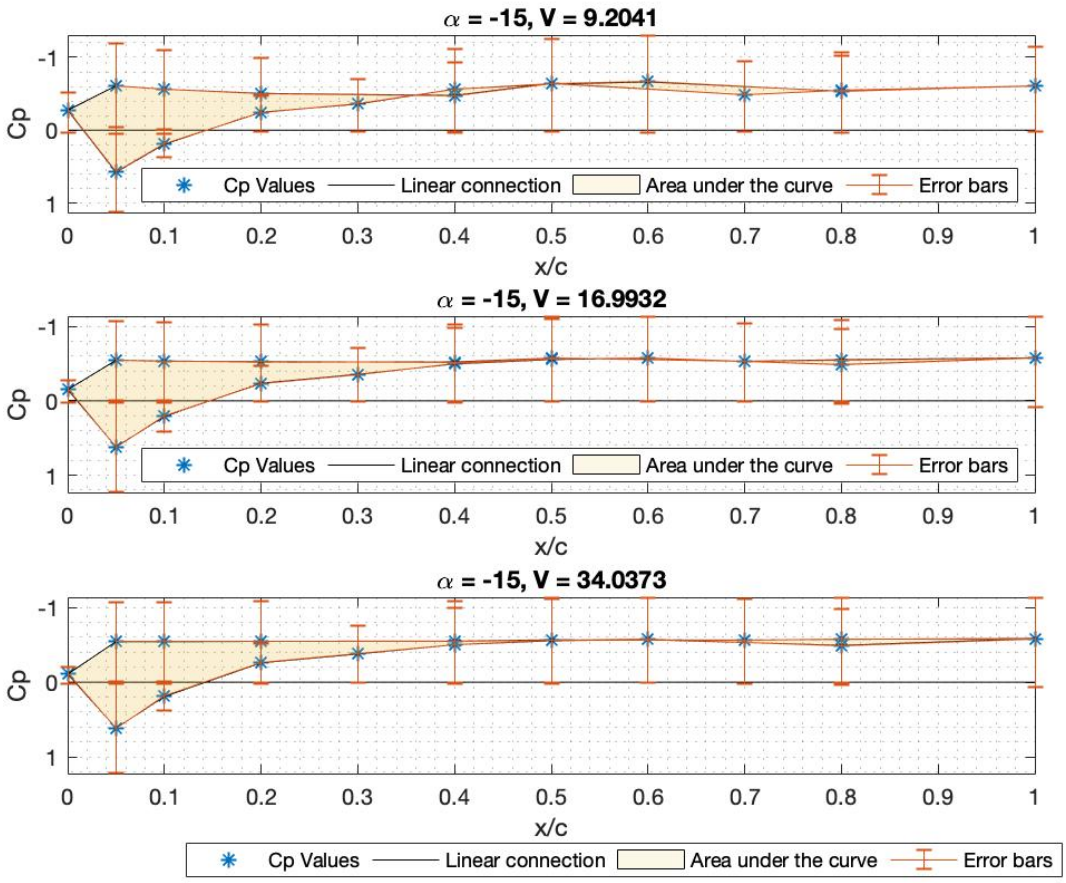

Fig. 11 Pressure coefficient versus normalized chord-wise position for different velocities at an angle of attack of negative 15 degrees

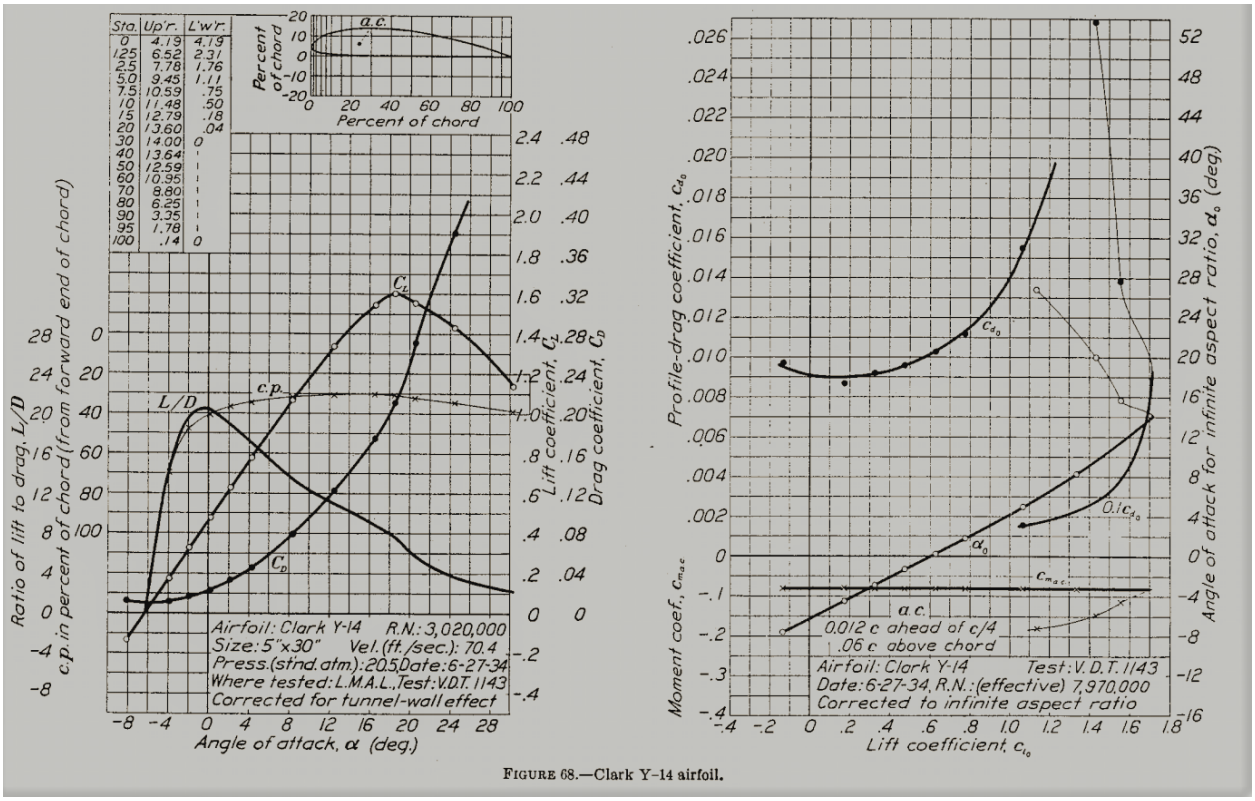

FIGURE 68.—Clark Y-14 airfoil.

Fig. 12 NACA Technical Report 628 graphs of Clark Y-14 Airfoil.

Table 1 Excluded Data

Section/Group	Data Point	Reason
S12 G1	9m/s @ 16 Degree AoA	Group did not record 9 m/s @ 16 Degree AoA
S11 G9	12 Degree AoA	Group used incorrect velocity 0, 9, 17 instead of 9, 17, 34
S14 G1	C_l/C_d	Bad value due to very small C_d